Frontiers of Information Technology & Electronic Engineering
www.jzus.zju.edu.cn; engineering.cae.cn; www.springerlink.com
ISSN 2095-9184 (print); ISSN 2095-9230 (online)
E-mail: jzus@zju.edu.cn

Exponential response electrical pole-changing method for a five-phase induction machine with a current sliding mode control strategy*

Jia-qiang YANG†‡, Rong-sen YIN, Xiao-jun ZHANG, Jin HUANG
(*College of Electrical Engineering, Zhejiang University, Hangzhou 310027, China*)
†E-mail: yjq1998@163.com

Received Nov. 21, 2016; Revision accepted Feb. 14, 2017; Crosschecked Aug. 14, 2017

Abstract: Electrical pole-changing technology leads to torque ripple and speed fluctuation despite broadening the constant power speed range of the multiphase induction machine (IM) system. To reduce the torque ripple and speed fluctuation of the machine, we investigate an exponential response electrical pole-changing method for five-phase IM with a current sliding-mode control strategy. This control strategy employs the dual-plane (d_1–q_1 and d_2–q_2) vector control method, which allows the IM to operate under different pole modes. Current sliding-mode controllers are applied instead of conventional proportional integral (PI) controllers to adjust the current vectors, and exponential current response achieves a smooth transition between the d_1–q_1 and d_2–q_2 planes. Compared with the step response pole-changing with PI control method, the proposed pole-changing method greatly reduces the torque ripple and speed fluctuation of the IM during the pole-changing process. Experimental results verify the exceptional performance of the proposed electrical pole-changing strategy.

Key words: Five-phase induction machine; Pole-change; Sliding-mode control; Exponential response; Torque ripple reduction
http://dx.doi.org/10.1631/FITEE.1601728 **CLC number:** TM346

1 Introduction

With development in modern power electronics technology and machine control theories, the inverter-fed driving technology of machines removes the limitation on the number of machine phases. Recent studies have increasingly focused on multiphase motors because of their advantages such as improved torque quality, smaller stator current per phase, reduced torque ripple, and increased fault tolerance. With these merits, multiphase machines are widely applied especially on ship propulsion, electric vehicle, and aerospace (Levi *et al*., 2007; 2016; Levi, 2008; 2016; Abdel-Khalik *et al.*, 2014; Mengoni *et al*., 2015; Barrero and Duran, 2016; Duran and Barrero, 2016; Subotic *et al.*, 2016). All of these applications require a high startup torque and a wide constant power speed range.

A multiphase machine possesses multiple control planes, including the fundamental current plane and harmonic current planes. Electrical pole-changing is a technology that can achieve the changing of multiphase machine's pole by changing the fundamental current and harmonic currents without power off. Electrical pole-changing can offer a high startup torque and a wide constant power speed range. Lipo and White (1991a; 1991b) and Lipo (1994) designed a six-phase machine coupling current model, which is equivalent to the two and four poles model. They achieved the 2/4 poles changing of the machine by changing the phase of the power supply current (Osama and Lipo, 1997). However, the torque of IM

‡ Corresponding author
* Project supported by the National Basic Research Program (973) of China (No. 2013CB035600)
ORCID: Jia-qiang YANG, http://orcid.org/0000-0002-3822-3301

significantly decreased during the pole-changing process. Kelly and Strangas (2007) and Ge *et al*. (2013) proposed three IM winding design schemes to achieve the transition from a 3-phase/12-pole model to a 9-phase/4-pole model. They also built a mathematical model of pole-phase modulation IM and a vector control system with fewer current sensors. However, the dynamic performance for pole-changing was not ideal. Aliabad *et al*. (2010) and Aliabad and Mirsalim (2012) proposed a pole-changing control strategy for the startup of a linear permanent magnet motor (Ershad *et al*., 2013). Simulation and experiment results verified that the pole-changing control strategy improves the torque and steady state performance of the linear permanent magnet motor. However, the speed decreased and the transition was not smooth during the pole-changing process. Tian *et al*. (2016) also investigated the pole-changing of a line-start permanent magnet synchronous motor which has a 6/8 pole-changing stator winding. A new structure of stator winding was designed to realize pole-changing. Wang *et al*. (2015; 2016a; 2016b) presented some research about the pole-changing permanent magnet memory machine. They designed and investigated a fractional slot pole-changing memory machine. The pole-changing permanent magnet machine was also applied to optimize the cogging torque. The major electromagnetic characteristics of serval optimization methods were compared in Wang *et al*. (2015). Li *et al*. (2016) designed and analyzed a variable-flux pole-changing flux-weakening DC-excited dual memory machine for electric vehicles. They improved the torque quality by injecting the fifth harmonic current under different magnetized levels of AlNiCo permanent motors. From the above studies, it is clear that the electrical pole-changing method is generally used to offer a high startup torque and a wide constant power speed range. Sometimes it is used to improve the torque quality and reduce the cogging torque by injecting harmonic current. Electrical pole-changing technology has broad application prospects in electric vehicles.

Studies on multiphase system transition theory (Jiang *et al*., 2003; Kelly, 2007; Gregor *et al*., 2010; Jones *et al*., 2012; Luis, 2014; Shi and Zhou, 2016) and multiphase machine vector control strategies (Abd Hafez *et al*., 2011; Duran *et al*., 2013; Hoang *et al*., 2015; Deng *et al.*, 2016) have greatly promoted the development of pole-changing technology. Step response electrical pole-changing with PI controllers between three and nine pairs of poles was achieved on a nine-phase IM. However, the load-carrying capacity of the IM was poor when running in the mode of nine pairs of poles. The IM also demonstrated high-speed fluctuation and torque ripple during the electrical pole-changing process. The exponential response electrical pole-changing with PI controllers between one and two pairs of poles was achieved on a five-phase IM. The five-phase IM load-carrying capacity was greatly improved. The speed fluctuation and torque ripple decreased during the pole-changing process. However, this technique is an indirect control method with a dynamic performance far from ideal (Dujic *et al*., 2011; Martin *et al.*, 2011).

Most of the abovementioned control systems employed PI controllers. However, the multiphase induction machine model includes integrator, oscillation, and unstable model parameters, especially in the electrical pole-changing process. In this application, a sliding-mode controller has its advantages in respects of rapid response and strong robustness. To improve the dynamic performance of electrical pole-changing, sliding-mode control (SMC) is introduced as an alternative.

Systems with sliding modes aim to constrain the system motion in a manifold. Slide planes have a rapid response and strong robustness because they can be designed, so they are not influenced by the variations in system parameters. Emelyanov proposed variable structure systems with sliding modes in the 1950s and Utkin made great contribution to the research in SMC (Utkin, 1977). Utkin *et al*. (1999) systematically studied SMC in electromechanical systems and promoted the development of SMC. Although early works on sliding modes mostly focused on dynamical systems in canonical form, recent sliding-mode methods have been applied in multiple-input multiple-output systems (Tuan *et al.*, 2013). Computers and digital signal processors are being widely used in modern industrial applications, and many control systems are discrete-time systems. Studies on the application of SMC in discrete-time systems have been conducted since 1980 (Gao *et al.*, 1995; Lee *et al.*, 2013).

In this paper, we introduce exponential response electrical pole-changing methods for five-phase IM with an SMC strategy. Given that five-phase IM

possesses two mutually decoupled control planes, namely, d_1-q_1 and d_2-q_2, the control strategy employs the dual-plane vector control method, which allows the IM to operate under different pole modes. Instead of PI controllers, current sliding-mode controllers are employed to adjust the current vectors. The exponential response is used to achieve the transition between d_1-q_1 and d_2-q_2 planes. This novel control strategy can reduce the torque ripple and speed fluctuation of the five-phase IM in the pole-changing process. This paper offers contributions in method and application. On the one hand, this paper is the first to combine exponential response and SMC in five-phase IM electrical pole-changing and has obtained a favorable performance. On the other hand, this paper provides an efficient solution for broadening the speed regulation extent of five-phase IM. The notations used in this paper are listed in Tables 1 and 2.

Table 1 Continuous variables and parameters of concern

Parameter	Description
c_1, c_2	Integral sliding mode coefficients
$\boldsymbol{C}_5$	Matrix of constant power transformation
e_{d1}, e_{q1}	Sliding mode reference variables
$\boldsymbol{I}_1$, $\boldsymbol{I}_2$	Vectors of fundamental harmonic current and second-order harmonic current
i_{sd1}, i_{sq1}	Components of d- and q-axis stator current vector on the d_1-q_1 plane
i_{rd1}, i_{rq1}	Components of d- and q-axis rotor current vector on the d_1-q_1 plane
i_{sd2}, i_{sq2}	Components of d- and q-axis stator current vector on the d_2-q_2 plane
i_{rd2}, i_{rq2}	Components of d- and q-axis rotor current vector on the d_2-q_2 plane
i_{sd1}^*, i_{sq1}^*	Reference values of excitation and torque current vector on the d_1-q_1 plane
i_{sd2}^*, i_{sq2}^*	Reference values of excitation and torque current vector on the d_2-q_2 plane
J	Moment of inertia
k_{sd1}, k_{sd2}	Excitation currents proportional constants
k_{sq1}, k_{sq2}	Torque currents proportional constants
L_{m1}, L_{s01}, L_{r01}	Stator magnetizing inductance, stator leakage inductance, and rotor leakage inductance on the d_1-q_1 plane
L_{m2}, L_{s02}, L_{r02}	Stator magnetizing inductance, stator leakage inductance, and rotor leakage inductance on the d_2-q_2 plane
L_{s1}, L_{r1}	Stator and rotor self-inductances of the fundamental harmonic
L_{s2}, L_{r2}	Stator and rotor self-inductances of the second-order harmonic
n	Number of IM phases
p	Differential operator
P_1, P_2	Pole-pair numbers of d_1-q_1 and d_2-q_2
R_{r1}, R_{r2}	Rotor resistances on d_1-q_1 and d_2-q_2 planes
s, s_1	Switching planes
s_{d1}, s_{q1}	Switching planes of d-axis and q-axis
T	Torque required to maintain IM speed
T_e	Electromagnetic torque of IM
T_{e1}, T_{e2}	Electromagnetic torques of the fundamental and second-order harmonic current
T_L	Load torque of IM
T_m	Total time of the pole-changing process
u_{sd1}, u_{sq1}	Components of d- and q-axis stator voltage on the d_1-q_1 plane
u_{sd2}, u_{sq2}	Components of d- and q-axis stator voltage on the d_2-q_2 plane
α_1, α_2, ε_1, ε_2, η_1, η_2	Controller gains
τ_{r1}, τ_{r2}	Rotor electromagnetic time constants
ψ_{rd1}, ψ_{rq1}	Flux linkages of d- and q-axis on the d_1-q_1 plane
ω_r	Rotor speed
ω_1, ω_2	Speed of rotor flux on d_1-q_1 and d_2-q_2 planes
ω_{s1}, ω_{s2}	Slip frequency of d_1-q_1 and d_2-q_2 planes
Δ	Boundary layer

Table 2 Discrete variables and parameters of concern

Parameter	Description
T_{sample}	Sampling time
k, k+1	Current step and next step
$\omega_1(k)$	Speed of rotor flux on the d_1-q_1 plane
$e_{d1}(k)$, $e_{q1}(k)$	Sliding mode reference variables of d- and q-axis for the current step
$e_{d1}(k+1)$, $e_{q1}(k+1)$	Sliding mode reference variables of d- and q-axis for the next step
$i_{sd1}(k)$, $i_{sq1}(k)$	Components of d- and q-axis stator current on the d_1-q_1 plane for the current step
$i_{sd1}(k+1)$, $i_{sq1}(k+1)$	Components of d- and q-axis stator current on the d_1-q_1 plane for the next step
$i_{sd1}^*(k)$, $i_{sq1}^*(k)$	Reference of excitation and torque current on the d_1-q_1 plane for the current step
$i_{sd1}^*(k+1)$, $i_{sq1}^*(k+1)$	Reference of excitation and torque current on the d_1-q_1 plane for the next step
$u_{sd1}(k)$, $u_{sq1}(k)$	Components of d- and q-axis stator voltage on the d_1-q_1 plane
$s(k)$, $s(k+1)$	Switching functions
$s_{d1}(k)$, $s_{q1}(k)$	Switching planes of d-axis and q-axis
ε, q, q_1, q_2	Controller gains

2 Structure and mathematical model of the five-phase induction machine

2.1 Structure of the five-phase induction machine

Among other multiphase systems, the five-phase machine system has captured wide attention and is considered an ideal alternative to the standard three-phase machine system. In the experiment five-phase IM with a symmetrically distributed winding is employed (spatial distribution angle is θ=2π/5). Fig. 1 presents the symmetrically distributed five-phase IM system scheme.

2.2 Mathematical model of the five-phase induction machine

The multi-phase IM system is a multivariable, coupled and nonlinear system. Mathematical models built on the electromechanical energy conversion principle are difficult to analyze. The current and voltage of the stator and rotor need to be transformed into the DC component to analyze the steady and transient states of multiphase IMs. For a five-phase symmetrical system, matrix $\boldsymbol{C}_5$ in Eq. (1) (see the bottom of this page) is used to transform the voltages and currents of the stator into a synchronous reference frame under a constant power condition.

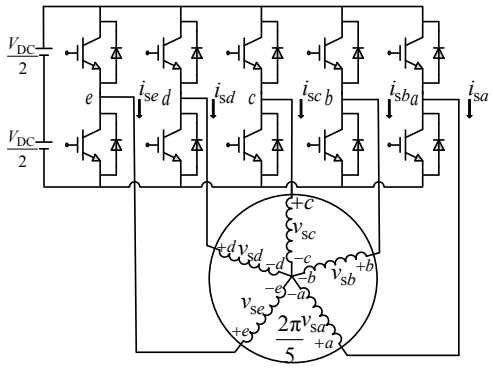

Fig. 1 Symmetrically distributed five-phase induction machine system

In Eq. (1), ξ=2π/5. $\boldsymbol{C}_5$ is an orthogonal matrix which comprises two pairs of d–q components. The first and second rows denote the d_1–q_1 subspace, and the third and fourth rows denote the d_2–q_2 subspace.

The mechanical equation of multiphase IM is expressed as follows:

$$T_{\text{e}} - T_{\text{L}} = J\frac{\text{d}}{\text{d}t}\omega_{\text{r}}. \tag{2}$$

The five-phase IM total electromagnetic torque equation is shown as follows:

$$T_{\text{e}} = P_1 L_{\text{m1}}(i_{sq1}i_{rd1} - i_{rq1}i_{sd1}) + P_2 L_{\text{m2}}(i_{sq2}i_{rd2} - i_{rq2}i_{rd2}). \tag{3}$$

Eqs. (1)–(3) transform the voltage and current of the stator of the winding symmetrically distributed machine into DC components in the d–q coordinate system. The equations of each d–q plane of multi-phase IM can be extracted independently.

$$\boldsymbol{C}_5 = \sqrt{\frac{2}{5}}\begin{bmatrix} \cos\varphi_1 & \cos(\varphi_1-\xi) & \cos(\varphi_1-2\xi) & \cos(\varphi_1-3\xi) & \cos(\varphi_1-4\xi) \\ -\sin\varphi_1 & -\sin(\varphi_1-\xi) & -\sin(\varphi_1-2\xi) & -\sin(\varphi_1-3\xi) & -\sin(\varphi_1-4\xi) \\ \cos\varphi_2 & \cos(\varphi_2-2\xi) & \cos(\varphi_2-4\xi) & \cos(\varphi_2-6\xi) & \cos(\varphi_2-8\xi) \\ -\sin\varphi_2 & -\sin(\varphi_2-2\xi) & -\sin(\varphi_2-4\xi) & -\sin(\varphi_2-6\xi) & -\sin(\varphi_2-8\xi) \\ \sqrt{2}/2 & \sqrt{2}/2 & \sqrt{2}/2 & \sqrt{2}/2 & \sqrt{2}/2 \end{bmatrix}. \tag{1}$$

For the five-phase IM, the voltage and torque equations of the fundamental harmonic current are expressed as Eq. (4) (see the bottom of this page) and Eq. (5):

$$T_{e1} = P_1 L_{m1}(i_{sd1} i_{rq1} - i_{rd1} i_{sq1}), \tag{5}$$

where $L_{s1}=L_{m1}+L_{s01}$, $L_{r1}=L_{m1}+L_{r01}$.

Similarly, the voltage and torque equations of the second-order harmonic are shown as Eq. (6) (see the bottom of this page) and Eq. (7):

$$T_{e2} = P_2 L_{m2}(i_{sd2} i_{rq2} - i_{rd2} i_{sq2}), \tag{7}$$

where $L_{s2}=L_{m2}+L_{s02}$, $L_{r2}=L_{m2}+L_{r02}$.

The sliding frequenies of d_1-q_1 and d_2-q_2 planes are calculated as follows:

$$\omega_{s1} = \omega_1 - \omega_r = \frac{L_{m1} i_{sq1}}{\tau_{r1} \psi_{rd1}}, \tag{8}$$

$$\omega_{s2} = \omega_2 - 2\omega_r = \frac{L_{m2} i_{sq2}}{\tau_{r2} \psi_{rd2}}. \tag{9}$$

Eqs. (4)–(9) reveal that the d_1–q_1 and d_2–q_2 planes can be controlled independently.

3 Principle of electrical pole-changing

For a multiphase IM with n phases, (n–1)/2 decoupled control planes are observed if n is odd. The phase current of multiphase IM can be transformed into (n–1)/2 decoupled planes by matrix. The principle of multiphase machine electrical pole-changing is to use the multi-control freedoms of the multiphase machine to generate the corresponding rotating magnetic field of the pole-pair number of the machine by controlling the phase current in a specific control plane.

Transformation between different rotating magnetic fields is an essential component of electrical pole-changing. By adopting a proper control strategy, the pole-pair number of a rotating magnetic field can be changed into another pole-pair number. In this way, we can achieve electrical pole-changing without cutting the power supply.

Two control freedoms are used because the five-phase IM possesses d_1–q_1 and d_2–q_2 orthogonal planes. Eqs. (1) and (4)–(7) show that the d_1–q_1 plane controls the fundamental harmonic current vector $\boldsymbol{I}_1$, while the d_2–q_2 plane controls the second-order harmonic current vector $\boldsymbol{I}_2$. Different current vectors correspond to different magnetic fields. The five-phase IM with $\boldsymbol{I}_1$ and $\boldsymbol{I}_2$ injection is equivalent to two three-phase IMs. Fundamental harmonic current $\boldsymbol{I}_1$ corresponds to a three-phase IM with one pair of poles, while the second-order harmonic current $\boldsymbol{I}_2$ corresponds to a three-phase IM with two pairs of poles. Fig. 2 presents the magnetic fields of d_1–q_1 and d_2–q_2.

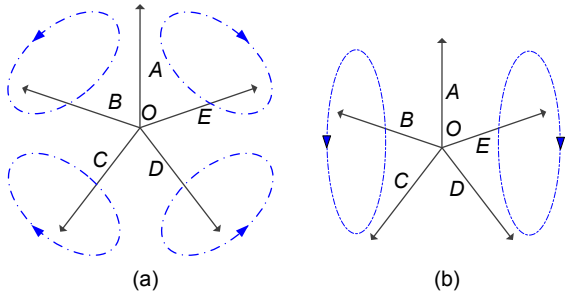

Fig. 2 Five-phase IM rotating magnetic fields: (a) two pairs of poles mode; (b) one pair of poles mode

$$\begin{bmatrix} u_{sd1} \\ u_{sq1} \\ 0 \\ 0 \end{bmatrix} = \begin{bmatrix} R_s + L_{s1}p & \omega_1 L_{s1} & L_{m1}p & \omega_1 L_{m1} \\ -\omega_1 L_{s1} & R_s + L_{s1}p & -\omega_1 L_{m1} & L_{m1}p \\ L_{m1}p & (\omega_1 - \omega_r)L_{m1} & R_{r1} + L_{r1}p & (\omega_1 - \omega_r)L_{r1} \\ -(\omega_1 - \omega_r)L_{m1} & L_{m1}p & -(\omega_1 - \omega_r)L_{r1} & R_{r1} + L_{r1}p \end{bmatrix} \begin{bmatrix} i_{sd1} \\ i_{sq1} \\ i_{rd1} \\ i_{rq1} \end{bmatrix}. \tag{4}$$

$$\begin{bmatrix} u_{sd2} \\ u_{sq2} \\ 0 \\ 0 \end{bmatrix} = \begin{bmatrix} R_s + L_{s2}p & \omega_2 L_{s2} & L_{m2}p & \omega_2 L_{m2} \\ -\omega_2 L_{s2} & R_s + L_{s2}p & -\omega_2 L_{m2} & L_{m2}p \\ L_{m2}p & (\omega_2 - 2\omega_r)L_{m2} & R_{r2} + L_{r2}p & (\omega_2 - 2\omega_r)L_{r2} \\ -(\omega_2 - 2\omega_r)L_{m2} & L_{m2}p & -(\omega_2 - 2\omega_r)L_{r2} & R_{r2} + L_{r2}p \end{bmatrix} \begin{bmatrix} i_{sd2} \\ i_{sq2} \\ i_{rd2} \\ i_{rq2} \end{bmatrix}. \tag{6}$$

Five-phase IM has the fundamental harmonic current $\boldsymbol{I}_1$ and the second-order harmonic current $\boldsymbol{I}_2$ at the same time during the electrical pole-changing process. The torques T_{e1} and T_{e2} produced by these currents are also changing. Given that the values of currents continuously change, a smooth electrical pole-changing transition can be achieved by ensuring the stability of total torque T_e.

4 Electrical pole-changing method

For the five-phase IM, the current vector controlled by different source voltage values and phases in d_1–q_1 and d_2–q_2 planes can independently generate the rotating magnetic field of one pair and two pairs of poles. Their corresponding torques are T_{e1} and T_{e2}. Pole-changing research must determine what kind of control strategy is employed to achieve a smooth transition between two different modes. In the pole-changing process, no torque break-off occurs and the torque ripple must be as small as possible.

4.1 Step response electrical pole-changing

A step response electrical pole-changing method is applied to a five-phase IM in this study. By employing the rotor field oriented control strategy, the stator current of the machine is divided into excitation currents i_{sd1}, i_{sd2} and torque currents i_{sq1}, i_{sq2}. These currents are switched over during the electrical pole-changing process.

At the beginning of the step response electrical pole-changing from one pair to two pairs of poles, the reference values of i_{sd1} and i_{sq1} immediately decrease from i_{sd1}^* and i_{sq1}^* to 0, while the reference values of i_{sd2} and i_{sq2} immediately increase from 0 to i_{sd2}^* and i_{sq2}^*. The real values of i_{sq1} and i_{sq2} change with delay during this pocess. The changes in the currents are shown as follows:

$$\begin{cases} i_{sd2}=i_{sd2}^*, \\ i_{sq2}=i_{sq2}^*, \\ i_{sd1}=0, \\ i_{sq1}=0. \end{cases} \tag{10}$$

The step response electrical pole-changing from two pairs to one pair of poles is illustrated as follows:

$$\begin{cases} i_{sd1}=i_{sd1}^*, \\ i_{sq1}=i_{sq1}^*, \\ i_{sd2}=0, \\ i_{sq2}=0. \end{cases} \tag{11}$$

Theoretically, the step response electrical pole-changing method has a very high transition speed. However, the real currents cannot change as fast as reference currents because of delays and dynamic processes. Therefore, this method generates torque ripples and speed fluctuations.

4.2 Exponential response electrical pole-changing

To reduce the torque ripple generated during the electrical pole-changing process via the step response method, an exponential response electrical pole-changing method is proposed. In the exponential response electrical pole-changing method, the torque and excitation currents are changed as presented in Eqs. (12) and (13), which represent the current transformation between the modes of one pair and two pairs of poles. The excitation current remains stable or slightly increases when the machine is unsaturated, which facilitates the reduction of torque fluctuation. The symbols k_{sd} and k_{sq} are factors of proportionality, which can regulate the relationship between actual current values and reference current values.

$$\begin{cases} i_{sd1}=k_{sd1}i_{sd1}^*, \\ i_{sq1}=k_{sq1}i_{sq1}^*\mathrm{e}^{-t/T_m}, \\ i_{sd2}=k_{sd2}i_{sd2}^*, \\ i_{sq2}=k_{sq2}i_{sq2}^*(1-\mathrm{e}^{-t/T_m}). \end{cases} \tag{12}$$

$$\begin{cases} i_{sd2}=k_{sd2}i_{sd2}^*, \\ i_{sq2}=k_{sq2}i_{sq2}^*\mathrm{e}^{-t/T_m}, \\ i_{sd1}=k_{sd1}i_{sd1}^*, \\ i_{sq1}=k_{sq1}i_{sq1}^*(1-\mathrm{e}^{-t/T_m}). \end{cases} \tag{13}$$

Fig. 3 presents the five-phase IM dual-plane vector control diagram with PI controllers. The d_1–q_1 and d_2–q_2 planes are controlled independently. The IM can run at either the d_1–q_1 or d_2–q_2 plane, controlled by switches 1 and 2. Switches are independent and can be both switched on. In this condition, the five-phase IM will operate with harmonic injection.

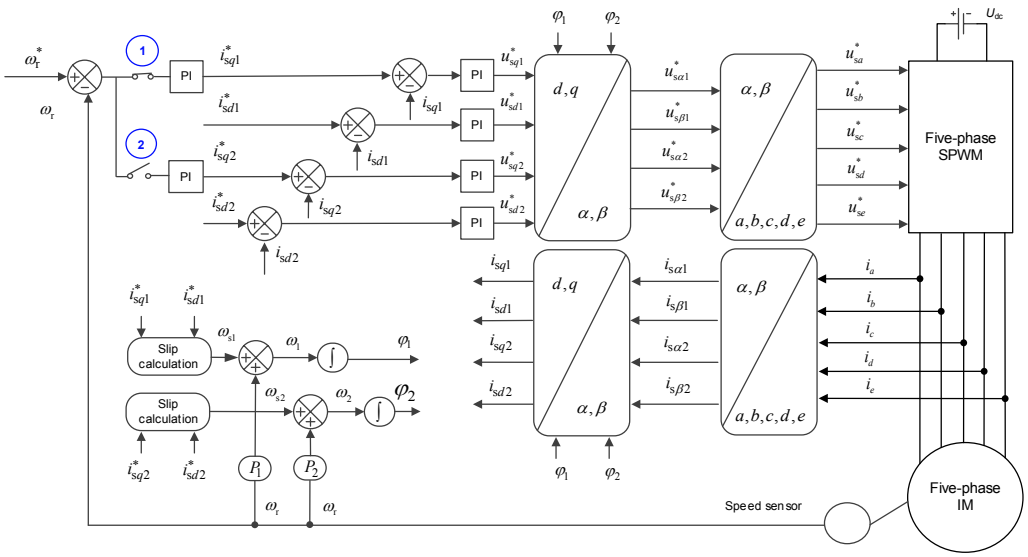

Fig. 3 Five-phase induction machine dual-plane vector control with PI controllers

5 Electrical pole-changing with sliding-mode variable structure control

Given their great steady-state and dynamic performance, PI controllers have been widely used in industrial control systems. However, the sliding-mode controller has its advantages in respects of rapid response and strong robustness for some objects that contain integrator, oscillation, and unstable model parameters, for example, the multiphase machine.

During the electrical pole-changing process, the five-phase machine contains the fundamental harmonic current, the second-order harmonic current, and unstable parameters. In this application, PI controllers have demonstrated poor performance in terms of tracking the current. To improve control precision, PI controllers must be upgraded or replaced. Sliding-mode variable structure controllers are used instead to control the current during the electrical pole-changing process. The sliding-mode variable structure controllers ensure the quick response of the system and overcome the poor robustness of PI controllers.

A multi-input vector sliding-mode variable structure controller is designed in this study according to the mathematical model of the five-phase IM. The d_1–q_1 and d_2–q_2 planes have the same SMC algorithms. We introduce the SMC algorithm of the d_1–q_1 plane as an example.

Rotor field oriented control is employed. The d–q coordinates are placed on synchronous rotating magnetic fields. Axis d is in the same direction of the rotor magnetic field. The following equation is obtained:

$$\begin{cases}\psi_{rd1}=\psi_{r1},\psi_{rq1}=0,\\ \psi_{r1}=\dfrac{L_{m1}i_{sd1}}{1+\tau_{r1}p}.\end{cases} \tag{14}$$

Under d–q synchronous rotating coordination, the fundamental harmonic current plane of the five-phase IM can be illustrated as

$$\begin{cases}-\dfrac{\mathrm{d}i_{sd1}}{\mathrm{d}t}=\dfrac{1}{\sigma L_s}\left(R_s+\dfrac{L_m^2}{L_r\tau_r}\right)i_{sd1}-\omega_1 i_{sq1}\\ \qquad\qquad -\dfrac{1}{\sigma L_{s1}}u_{sd1}-\dfrac{R_{r1}}{\sigma L_{s1}L_{r1}}\psi_{rd1},\\ -\dfrac{\mathrm{d}i_{sq1}}{\mathrm{d}t}=\omega_1 i_{sd1}+\dfrac{R_{s1}}{\sigma L_{s1}}i_{sq1}+\dfrac{1}{\sigma L_{s1}}u_{sq1}+\omega_1\dfrac{L_{m1}}{\sigma L_{s1}L_{r1}}\psi_{rd1},\\ \dfrac{\mathrm{d}\psi_{rd1}}{\mathrm{d}t}=\dfrac{L_{m1}}{\tau_{r1}}i_{sd1}-\dfrac{1}{\tau_{r1}}\psi_{rd1},\\ \psi_{rq1}=0.\end{cases} \tag{15}$$

Based on this mathematical model, a multi-input vector sliding-mode variable structure controller is designed, by which i_{sd} and i_{sq} can quickly reach the given values. The sliding-mode reference variables are presented as follows:

$$x_1=\begin{bmatrix}e_{d1}\\ e_{q1}\end{bmatrix}=\begin{bmatrix}i^*_{sd1}-i_{sd1}\\ i^*_{sq1}-i_{sq1}\end{bmatrix}. \tag{16}$$

The dynamic SMC variables are designed:

$$u_1=\begin{bmatrix}u_{sd1}\\ u_{sq1}\end{bmatrix}. \tag{17}$$

Combined with the above formulae, the sliding-mode state equation, $\dot{X}=AX+Bu+e$, can be presented as Eq. (18) (see the bottom of this page).

According to Eq. (14), the rotor excitation flux of the multiphase induction machine is a low-pass first-order filter of stator excitation current, which can be regarded as having little change.

Two sliding-mode planes, namely, s_{d1} and s_{q1}, are defined as follows:

$$s_1=\begin{bmatrix}s_{d1}\\ s_{q1}\end{bmatrix}=\begin{bmatrix}c_1\int_0^t e_{d1}\mathrm{d}t+e_{d1}\\ c_2\int_0^t e_{q1}\mathrm{d}t+e_{q1}\end{bmatrix}. \tag{19}$$

c_1 and c_2 are sliding-mode surface integral coefficients of d- and q-axis and c_1>0, c_2>0. The exponential approach law is designed as Eq. (20):

$$\dot{s}_1=\begin{bmatrix}\dot{s}_{d1}\\ \dot{s}_{q1}\end{bmatrix}=\begin{bmatrix}-\varepsilon_1\operatorname{sgn}(s_{d1})-\eta_1 s_{d1}\\ -\varepsilon_2\operatorname{sgn}(s_{q1})-\eta_2 s_{q1}\end{bmatrix}. \tag{20}$$

In the sliding surface, $\dot{s}=s=0$. Then the current SMC law of the five-phase IM can be presented as Eq. (21) (see the bottom of this page).

Consider a Lyapunov function candidate as follows:

$$L=\frac{1}{2}s^2. \tag{22}$$

The Lyapunov stability of SMC can be proved as Eq. (23) (see the bottom of this page). According to Eq. (23), the SMC system is stable in a large range, when ε_1 and ε_2 satisfy the following conditions:

$$\begin{cases}\varepsilon_1>\dfrac{1}{\sigma L_{s1}}\left(R_{s1}+\dfrac{L_{m1}^2}{L_{r1}\tau_{r1}}\right)i^*_{sd1}-\omega_1 i^*_{sq1}-\dfrac{L_{m1}}{\sigma L_{s1}L_{r1}\tau_{r1}}\psi_{rd1},\\ \varepsilon_2>\omega_1 i^*_{sd1}+\dfrac{R_{s1}}{\sigma L_{s1}}i^*_{sq1}+\omega_1\dfrac{L_{m1}}{\sigma L_{s1}L_{r1}}\psi_{rd1}.\end{cases} \tag{24}$$

To solve the buffeting problem caused by the sliding-mode variable structure controller, the discontinuous function sgn(s) can be replaced by the

$$\begin{aligned}\begin{bmatrix}\dot{e}_{d1}\\ \dot{e}_{q1}\end{bmatrix}=&\begin{bmatrix}-\dfrac{1}{\sigma L_{s1}}\left(R_{s1}+\dfrac{L_{m1}^2}{L_{r1}\tau_{r1}}\right) & \omega_1\\ -\omega_1 & -\dfrac{R_{s1}}{\sigma L_{s1}}\end{bmatrix}\begin{bmatrix}e_d\\ e_q\end{bmatrix}+\begin{bmatrix}-\dfrac{1}{\sigma L_{s1}} & 0\\ 0 & -\dfrac{1}{\sigma L_{s1}}\end{bmatrix}\begin{bmatrix}u_{sd1}\\ u_{sq1}\end{bmatrix}\\ &+\begin{bmatrix}\dfrac{1}{\sigma L_{s1}}\left(R_{s1}+\dfrac{L_{m1}^2}{L_{r1}\tau_{r1}}\right)i^*_{sd1}-\omega i^*_{sq1}-\dfrac{L_{m1}}{\sigma L_{s1}L_{r1}\tau_{r1}}\psi_{rd1}\\ \omega_1 i^*_{sd1}+\dfrac{R_{s1}}{\sigma L_{s1}}i^*_{sq1}+\omega_1\dfrac{L_{m1}}{\sigma L_{s1}L_{r1}}\psi_{rd1}\end{bmatrix}.\end{aligned} \tag{18}$$

$$\boldsymbol{u}_1=\begin{bmatrix}u_{sd1}\\ u_{sq1}\end{bmatrix}=\begin{bmatrix}\left(\sigma L_{s1}c_1-R_{s1}-\dfrac{L_{m1}^2}{L_{r1}\tau_{r1}}\right)e_{d1}+\omega_1\sigma L_{s1}e_{q1}+\varepsilon_1\sigma L_{s1}\operatorname{sgn}(s_{d1})+\eta_1\sigma L_{s1}s_{d1}\\ (\sigma L_{s1}c_2-R_{s1})e_{q1}-\omega_1\sigma L_{s1}e_{d1}+\varepsilon_2\sigma L_{s1}\operatorname{sgn}(s_{q1})+\eta_2\sigma L_{s1}s_{q1}\end{bmatrix}. \tag{21}$$

$$\begin{aligned}\dot{L}&=s_{d1}\dot{s}_{d1}+s_{q1}\dot{s}_{q1}=s_{d1}(c_1e_{d1}+\dot{e}_{d1})+s_{q1}(c_2e_{q1}+\dot{e}_{q1})\\ &\le-|s_{d1}|\left[\varepsilon_1-\frac{1}{\sigma L_{s1}}\left(R_{s1}+\frac{L_{m1}^2}{L_{r1}\tau_{r1}}\right)i^*_{sd1}-\omega i^*_{sq1}-\frac{L_{m1}}{\sigma L_{s1}L_{r1}\tau_{r1}}\psi_{rd1}\right]\\ &\quad-|s_{q1}|\left(\varepsilon_2-\omega_1 i^*_{sd1}+\frac{R_{s1}}{\sigma L_{s1}}i^*_{sq1}+\omega_1\frac{L_{m1}}{\sigma L_{s1}L_{r1}}\psi_{rd1}\right)-\eta_1 s_{d1}^2-\eta_2 s_{q1}^2.\end{aligned} \tag{23}$$

following continuous saturation function:

$$\mathrm{sat}(s)=\begin{cases}+1, & s>\Delta,\\ ks, & |s|\le\Delta,\\ -1, & s<-\Delta,\end{cases} \tag{25}$$

where Δ represents the boundary layer, and $\Delta\cdot k$=1. The d–q reference voltage equations are

$$\begin{cases}u_{sd1}=\left(\sigma L_{s1}c_1-R_{s1}-\dfrac{L_{m1}^2}{L_{r1}\tau_{r1}}\right)e_{d1}+\omega_1\sigma L_{s1}e_{q1}\\ \qquad +\varepsilon_1\sigma L_{s1}\,\mathrm{sat}(s_{d1})+\eta_1\sigma L_{s1}s_{d1},\\ u_{sq1}=(\sigma L_{s1}c_2-R_{s1})e_{q1}-\omega_1\sigma L_{s1}e_{d1}\\ \qquad +\varepsilon_2\sigma L_{s1}\,\mathrm{sat}(s_{q1})+\eta_2\sigma L_{s1}s_{q1}.\end{cases} \tag{26}$$

After entering the sliding state, if the system is stable in the sliding plane, s_1=s_2=0 can be obtained:

$$\begin{cases}i_{sd1}=i_{sd1}^*,\\ i_{sq1}=i_{sq1}^*.\end{cases} \tag{27}$$

In the experiments, a DSP is employed to control the five-phase IM. Therefore, the control function should be discretized to be applied to the DSP control system. For the experiment system, the sampling frequency is 10 kHz and the sampling time T_{sample} is 0.0001 s. Similarly, set it as a continuous system. The error state equation of the discrete time systems is shown as Eq. (28) (see the bottom of this page).

The discrete reaching law is shown as Eq. (29):

$$\frac{s(k+1)-s(k)}{T_{\mathrm{sample}}}=-\varepsilon\,\mathrm{sgn}(s(k))-qs(k), \tag{29}$$

where ε>0, q>0, and qT_{sample}<1.

The discrete system is Lyapunov stable, when $|s(k)|$ satisfies the following conditions:

$$|s(k)|>\frac{\varepsilon T_{\mathrm{sample}}}{2-qT_{\mathrm{sample}}}. \tag{30}$$

Then the control function with sat(s) of the discrete system can be obtained as Eq. (31) (see the bottom of this page).

Fig. 4 presents the schematic of the exponential response electrical pole-changing methods for the five-phase IM with the SMC strategy. The torque allocation block is illustrated in Eqs. (32) and (33):

$$T^*=\frac{T_{e1}^*+T_{e2}^*}{2}+f(x)\left(\frac{1}{2}-\frac{t}{T_m}\right)(T_{e1}^*-T_{e2}^*), \tag{32}$$

$$f(x)=\begin{cases}1, & 1\text{ pair to }2\text{ pairs},\\ -1, & 2\text{ pairs to }1\text{ pair}.\end{cases} \tag{33}$$

6 Experimental results

6.1 Experimental platform

Several experiments have been conducted on a set of five-phase IM system platforms to validate the proposed algorithm. Fig. 5a shows the schematic of the five-phase IM system.

$$\begin{bmatrix}e_{d1}(k+1)\\ e_{q1}(k+1)\end{bmatrix}=\begin{bmatrix}1-\dfrac{T_{\mathrm{sample}}}{\sigma L_{s1}}\left(R_{s1}+\dfrac{L_{m1}^2}{L_{r1}\tau_{r1}}\right) & T_{\mathrm{sample}}\omega_1(k)\\ -T_{\mathrm{sample}}\omega(k) & 1-T_{\mathrm{sample}}\dfrac{R_{s1}}{\sigma L_{s1}}\end{bmatrix}\begin{bmatrix}e_{d1}(k)\\ e_{q1}(k)\end{bmatrix}-\frac{T_{\mathrm{sample}}}{\sigma L_{s1}}\begin{bmatrix}u_{sd1}(k)+\dfrac{R_{r1}}{L_{r1}}\psi_{rd1}\\ -u_{sq1}(k)-\omega_1(k)\dfrac{L_{m1}}{L_{r1}}\psi_{rd1}\end{bmatrix}$$
$$+\begin{bmatrix}-1+\dfrac{T_{\mathrm{sample}}}{\sigma L_{s1}}\left(R_{s1}+\dfrac{L_{m1}^2}{L_{r1}\tau_{r1}}\right) & -T_{\mathrm{sample}}\omega_1(k)\\ T_{\mathrm{sample}}\omega_1(k) & -1+T_{\mathrm{sample}}\dfrac{R_{s1}}{\sigma L_{s1}}\end{bmatrix}\begin{bmatrix}i_{sd1}^*(k)\\ i_{sq1}^*(k)\end{bmatrix}+\begin{bmatrix}i_{sd1}^*(k+1)\\ i_{sq1}^*(k+1)\end{bmatrix}. \tag{28}$$

$$\begin{cases}u_{sd1}(k)=\left[\dfrac{\sigma L_{s1}}{T_{\mathrm{sample}}}-\left(R_{s1}+\dfrac{L_{m1}^2}{L_{r1}\tau_{r1}}\right)\right]e_{d1}(k)+\sigma L_{s1}\omega_1(k)e_{q1}(k)+\dfrac{\sigma L_{s1}}{T_{\mathrm{sample}}}\left[(1-qT_{\mathrm{sample}})s_{d1}(k)-\varepsilon_1T_{\mathrm{sample}}\,\mathrm{sat}(s_{d1}(k))\right],\\ u_{sq1}(k)=-\sigma L_{s1}\omega_1(k)e_{d1}(k)+\left(\dfrac{\sigma L_{s1}}{T_{\mathrm{sample}}}-R_{s1}\right)e_{q1}(k)+\dfrac{\sigma L_{s1}}{T_{\mathrm{sample}}}\left[(1-qT_{\mathrm{sample}})s_{q1}(k)-\varepsilon_2T_{\mathrm{sample}}\,\mathrm{sat}(s_{q1}(k))\right].\end{cases} \tag{31}$$

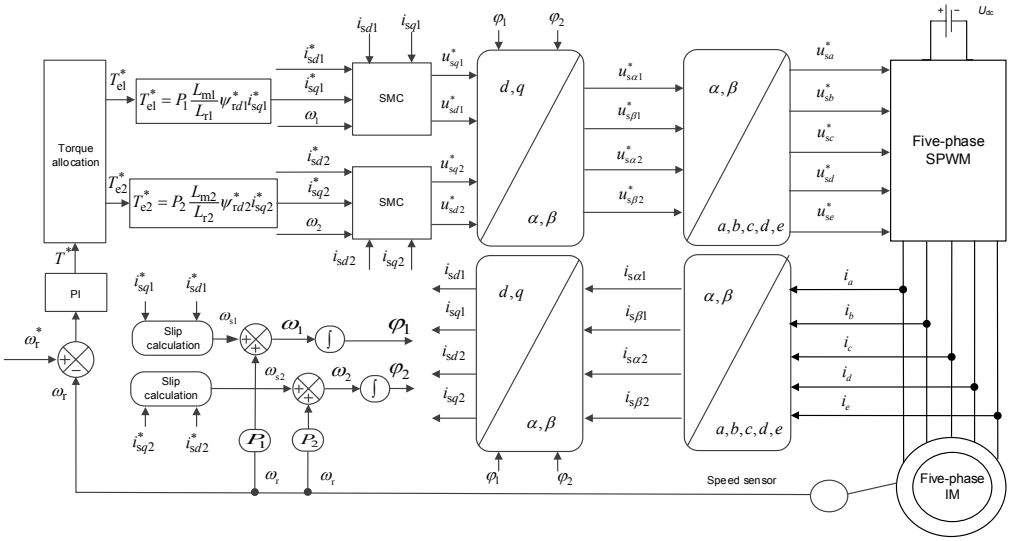

Fig. 4 Schematic of five-phase induction machine sliding-mode variable structure control

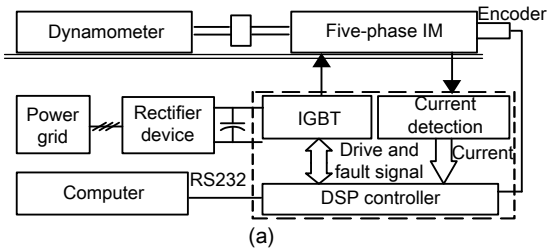

(a)

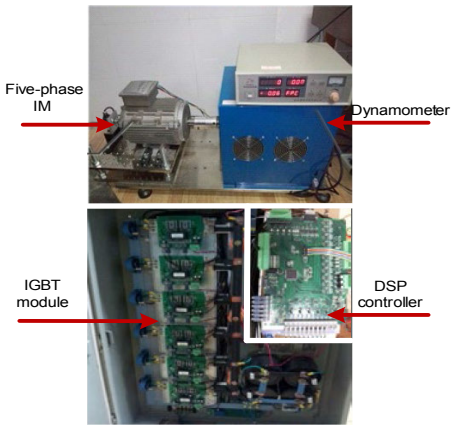

(b)

Fig. 5 Five-phase induction machine system experimental platform: (a) experimental platform schematic; (b) experimental device

Table 3 shows the parameters of the five-phase IM, while Fig. 5b shows the structure diagram of the experimental platform. The system comprises five-phase IM, the IGBT driver module, the hysteresis dynamometer, and the DSP 28335 master controller. The switching frequency is set to 10 kHz in the experiments.

6.2 Dual-plane vector control

The basis of electrical pole-changing is that the five-phase IM can be operated stably and independently in the d_1–q_1 and d_2–q_2 planes. Fig. 6 shows the phase current and electromagnetic torque waveform of the five-phase IM during its stable operation in the d_1–q_1 plane. The rated speed is 1500 r/min and the load torque is 10 N·m. The phase current and electromagnetic torque waveforms of the five-phase IM are illustrated in Figs. 6a and 6b. Both of these waveforms are under one pair of poles mode.

Table 3 The five-phase induction machine parameters

Parameter	Value
Power	3 kW
Nominal phase voltage	155 V
Stator resistance, R_s	1.28 Ω
FH rotor resistance, R_{r1}	0.4651 Ω
FH excitation inductance, L_{m1}	0.2504 H
FH stator leakage inductance, L_{s01}	0.0063 H
FH rotor leakage inductance, L_{r01}	0.0103 H
Nominal phase current	7 A
Number of pole-pairs	1 or 2
SH rotor resistance, R_{r2}	0.5427 Ω
SH excitation inductance, L_{m2}	0.0644 H
SH stator leakage inductance, L_{s02}	0.0067 H
SH rotor leakage inductance, L_{r02}	0.0079 H

FH: fundamental harmonic; SH: second-order harmonic

Fig.7 shows the waveforms of the phase current and electromagnetic torque of the five-phase IM when it runs stably in the d_2-q_2 plane. The rated speed is

1500 r/min and the load torque is 10 N·m. Both of these waveforms are obtained under two pairs of poles mode.

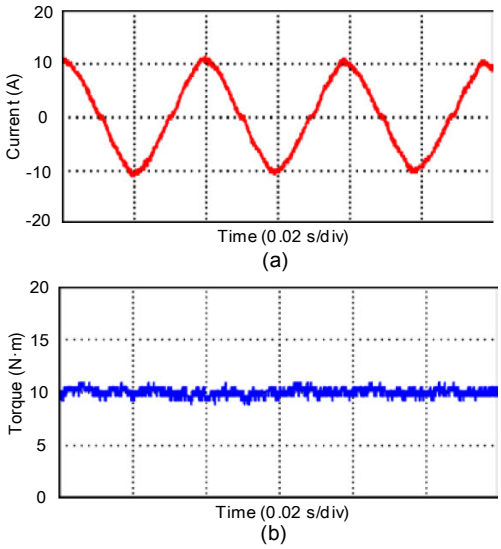

Fig. 6 Phase current and torque of the d_1-q_1 plane: (a) phase current waveform; (b) torque waveform

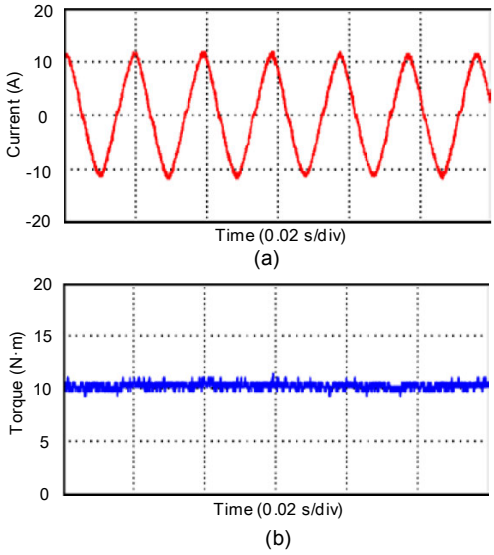

Fig. 7 Phase current and torque of the d_2-q_2 plane: (a) phase current waveform; (b) torque waveform

Fig. 6a shows that when running at the rated speed 1500 r/min, the phase current frequency of the one pair of poles mode is 25 Hz, while Fig. 7a shows that the phase current frequency of the two pairs of poles mode is 50 Hz. The frequency of the two pairs of poles mode is twice as much as that of the one pair of poles mode, which meets the machine speed formula n=60f/P. The torque waveforms of both modes are stable, which indicates that the machine can run steadily and independently in the one pair and two pairs of poles modes.

Given the limitation in space, we will present only the experiment results of electrical pole-changing from two pairs of poles mode to one pair of poles mode. Similar results are obtained for the opposite direction (i.e., from one pair of poles mode to two pairs of poles mode) and will not be discussed in this study.

6.3 Step response electrical pole-changing with PI controllers

Figs. 8–11 show the waveforms of the phase current, speed, torque, and torque current of the five-phase IM when the machine is changing from two pairs of poles mode to one pair of poles mode via step response electrical pole-changing with PI control. In the experiment, the speed is set to 1500 r/min, while the load torque is set to 10 N·m. Fig. 8a shows the waveform of the phase current of the five-phase machine under step response electrical pole-changing with PI control, while Fig. 8b shows the partial enlargement of the phase current waveform during the pole-changing process. The phase current decreases from 12 A to 5 A and then increases to 16 A, while its amplitude is gradually attenuated.

Fig. 9 illustrates the speed waveform of the machine under step response electrical pole-changing with PI control. Corresponding to the phase current waveform during the pole-changing process, the speed of the machine decreases from 1500 r/min to 800 r/min in no more than 0.2 s before gradually returning to its initial value.

Fig. 10 shows the electromagnetic torque waveform under step response pole-changing with PI control. The electromagnetic torque sharply decreases from 10 N·m to 5 N·m at the beginning of the pole-changing process. Afterward, the torque starts to increase steadily and overshoots slightly at the maximum value of approximately 12.5 N·m before returning to its initial value of 10 N·m.

Fig. 11 shows the waveforms of torque currents i_{sq1} and i_{sq2} in dual planes. At the beginning of the pole-changing process, i_{sq2} instantly drops to 0, while i_{sq1} gradually increases, overshoots with the maximum value of 13 A, and eventually becomes stable.

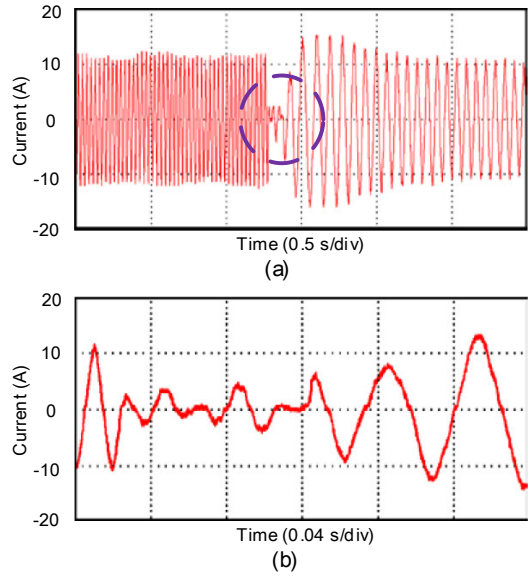

Fig. 8 Step response pole-changing phase current: (a) phase current waveform; (b) partial enlargement of the phase current waveform

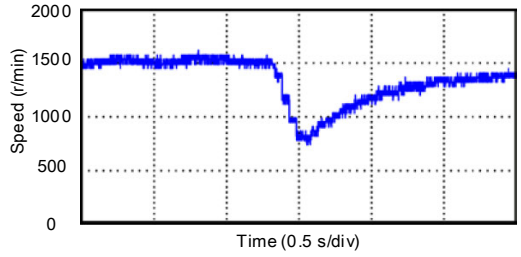

Fig. 9 Waveform of speed under step response pole-changing

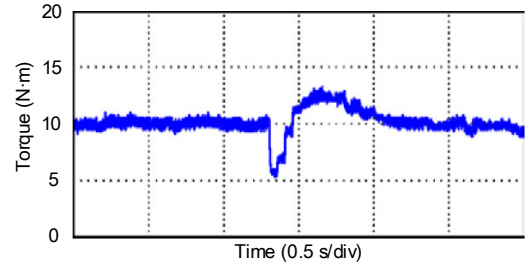

Fig. 10 Waveform of torque under step response pole-changing

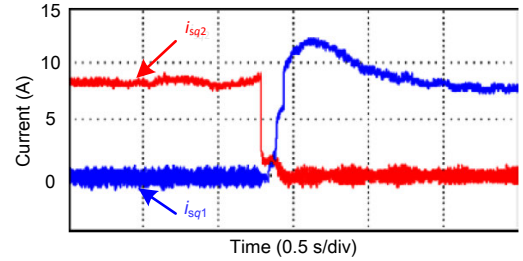

Fig. 11 Waveforms of i_{sq1} and i_{sq2} under step response pole-changing

Figs. 8–11 illustrate that both the electromagnetic torque and speed decrease sharply in the pole-changing process under step response pole-changing with PI control. The pole-changing process is not smooth.

6.4 Exponential response electrical pole-changing with PI controllers

Figs. 12–15 show the phase current, speed, torque, and torque current waveforms of the five-phase IM when the machine is changing from two pairs of poles mode to one pair of poles mode by exponential response electrical pole-changing with PI control. In the experiment, the speed is set to 1500 r/min and the load torque is set to 10 N·m.

Fig. 12a shows the waveform of the phase current of the five-phase IM under exponential response electrical pole-changing with PI control, while Fig.12b shows the partial enlargement of the phase current waveform during the pole-changing process. The degree of the exponential response phase current amplitude attenuation during the electrical pole-changing process is less than that during the step response pole-changing process.

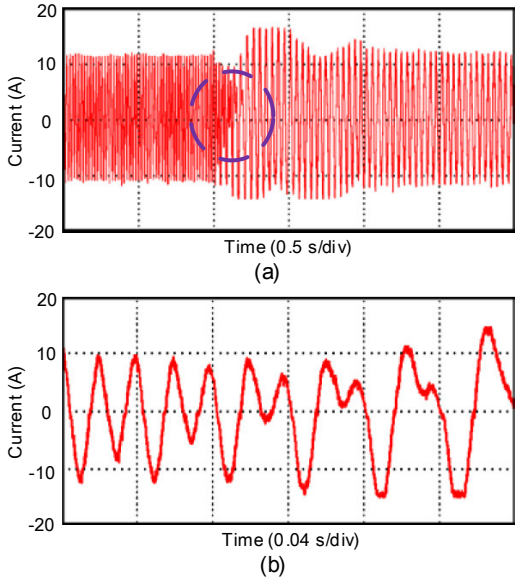

Fig. 12 Exponential response pole-changing phase current: (a) phase current waveform; (b) partial enlargement of the phase current waveform

Fig. 13 illustrates the IM speed waveform under exponential response electrical pole-changing with PI control. Corresponding to the phase current waveform

during the pole-changing process, the machine speed ripple is also greatly reduced by about 50 r/min as compared to the speed ripple of step response electrical pole-changing.

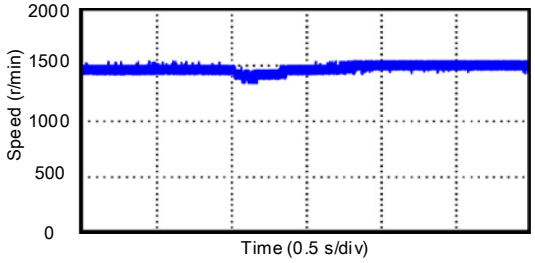

Fig. 13 Waveform of speed under exponential response pole-changing

Fig. 14 illustrates the electromagnetic torque waveform under exponential response pole-changing with PI control. The electromagnetic torque generally remains stable when compared to its counterpart in step response. The electromagnetic torque decreases by 2.5 N·m to its lowest value of 7.5 N·m before increasing to 11 N·m. The electromagnetic torque does not return to 10 N·m within the range shown in Fig. 14.

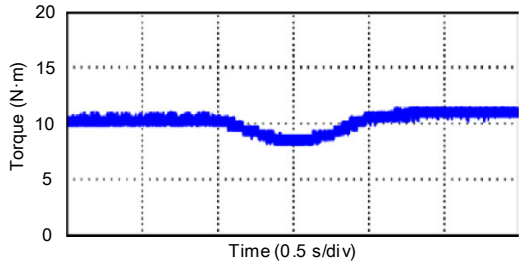

Fig. 14 Waveform of torque under exponential response pole-changing

Fig. 15 illustrates the waveforms of torque current i_{sq1} and i_{sq2} in dual planes of the exponential response electrical pole-changing process. At the beginning of pole-changing, i_{sq2} smoothly damps to 0 through the exponential response. By contrast, i_{sq1} increases gradually through slope response, overshoots with the maximum value of 9.5 A, and eventually becomes stable. The overshoots of i_{sq1} can lead to fluctuations in the torque and speed of the machine.

6.5 Exponential response electrical pole-changing with SMC controllers

Figs. 16–19 show the waveforms of the phase current, speed, torque, and torque current of the five-phase IM when the mode of the machine changes from two pairs of poles to one pair of poles by exponential response electrical pole-changing with SMC control. In the experiment, the speed is set to 1500 r/min and the load torque is set to 10 N·m.

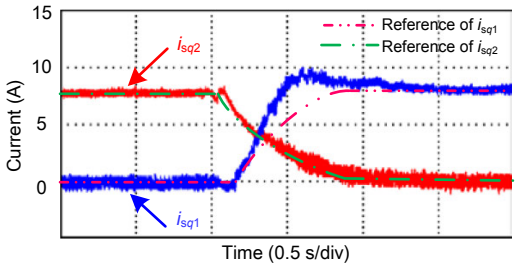

Fig. 15 Waveforms of i_{sq1} and i_{sq2} under exponential response pole-changing

Fig. 16a shows the phase current waveform of the five-phase IM under exponential response electrical pole-changing with SMC control, while Fig. 16b shows the partial enlargement of the phase current waveform during the pole-changing process. The exponential response phase current amplitude attenuation degree in the electrical pole-changing process is less than that in the exponential response pole-changing process with PI control.

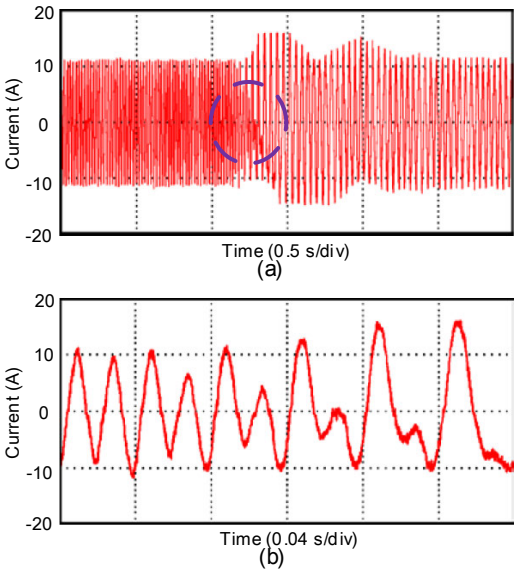

Fig. 16 Exponential response pole-changing with SMC control phase current: (a) phase current waveform; (b) partial enlargement of the phase current waveform

Fig. 17 illustrates the machine speed waveform under exponential response electrical pole-changing

with SMC control. The fluctuation in machine speed is also greatly reduced to 20 r/min as compared to the speed ripple of exponential response electrical pole-changing with PI control.

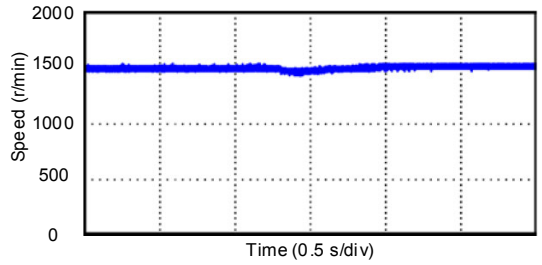

Fig. 17 Waveform of speed under exponential response pole-changing with SMC control

Fig. 18 shows the electromagnetic torque waveform under exponential response pole-changing with SMC control. The electromagnetic torque remains stable as compared to its counterpart in step response. The electromagnetic torque also slightly decreases by 1 N·m, reaches the lowest value of 9 N·m, and eventually returns to its initial value of 10 N·m.

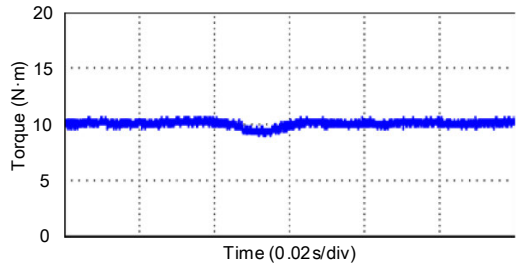

Fig. 18 Waveform of torque under exponential response pole-changing with SMC control

Fig. 19 shows the waveforms of torque currents i_{sq1} and i_{sq2} in the dual planes of exponential response electrical pole-changing with SMC control. At the beginning of the pole-changing process, both i_{sq1} and i_{sq2} smoothly change through the exponential response. i_{sq1} decreases gradually to 0, while i_{sq2} increases steadily to 8 A. No overshoot of i_{sq1} has been observed.

To compare their influence on the electrical pole-changing of SMC control and traditional PI control, the stator flux linkage waveforms of pole-changing with both control strategies are presented in Fig. 20.

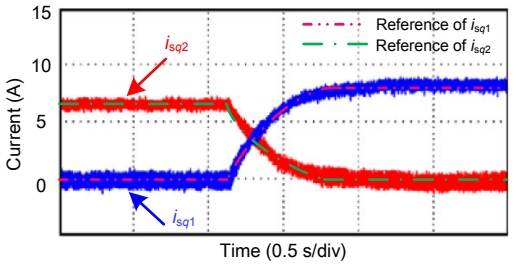

Fig. 19 Waveforms of i_{sq1} and i_{sq2} under exponential response pole-changing with SMC control

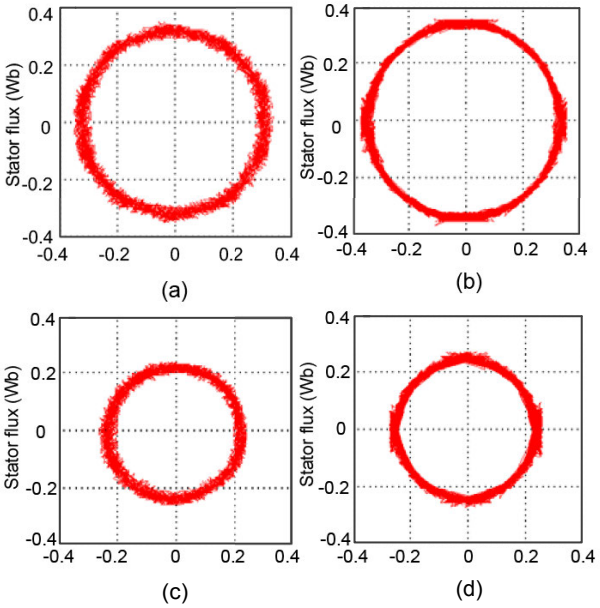

Fig. 20 Stator flux linkage of different modes: (a) one pair of poles with PI control; (b) one pair of poles with SMC control; (c) two pairs of poles with PI control; (d) two pairs of poles with SMC control

Figs. 20a–20d show the stator flux linkage waveforms of pole-changing with both PI and SMC strategies under the two modes of one and two pairs of poles. When an appropriate boundary layer is employed, the SMC control strategy can reduce the stator flux fluctuation much better than the PI control strategy. Fig. 20 shows that the boundary of the magnetic chain round is smoother and has fewer burrs. The decrease in stator flux fluctuation can improve the smoothness of the pole-changing process.

The above experiments show that the exponential response electrical pole-changing process with the SMC control strategy has a superior control performance and can greatly reduce the torque and speed fluctuation of the five-phase machine.

7 Conclusions

In this paper, we have presented a detailed comparison of several five-phase IM pole-changing methods and proposed exponential response electrical pole-changing methods for five-phase IM with the current SMC strategy. The step response pole-changing with PI control will cause fluctuation in electromagnetic torque and speed during the five-phase electrical pole-changing process. The PI controller results in electromagnetic torque fluctuation and speed drop because of current delay. To eliminate the negative effect of step response and the PI controller, we have proposed exponential response electrical pole-changing with the SMC control strategy. The performance of this strategy has been verified through extensive experiments. The proposed method can be regarded as valuable references to electrical pole-changing study.

References

Abdel-Khalik, A.S., Daoud, M.I., Ahmed, S., *et al*., 2014. Parameter identification of five-phase induction machines with single layer windings. *IEEE Trans. Ind. Electron.*, **61**(10):5139-5154. https://doi.org/10.1109/TIE.2013.2297294

Abd Hafez, A.A., Todd, R., Forsyth, A.J., *et al.*, 2011. Direct current ripple compensation for multi-phase fault-tolerant machines. *IET Electr. Power Appl.*, **5**(1):28-36. https://doi.org/10.1049/iet-epa.2009.0217

Aliabad, A.D., Mirsalim, M., 2012. Analytic modeling and dynamic analysis of pole-changing line-start permanent-magnet motors. *IET Electr. Power Appl.*, **6**(3):149-155. https://doi.org/10.1049/iet-epa.2011.0146

Aliabad, A.D., Mirsalim, M., Ershad, N.F., 2010. Line-start permanent-magnet motors: significant improvements in starting torque, synchronization, and steady-state performance. *IEEE Trans. Magn*., **46**(12):4066-4072. https://doi.org/10.1109/TMAG.2010.2070876

Barrero, F., Duran, M.J., 2016. Recent advances in the design, modeling and control of multiphase machines—part 1. *IEEE Trans. Ind. Electron*., **63**(1):449-458. https://doi.org/10.1109/TIE.2015.2447733

Deng, Y., Wang, Y.B., Teo, K.H., *et al*., 2016. A simplified space vector modulation scheme for multilevel converters. *IEEE Trans. Power Electron*., **31**(3):1873-1886. https://doi.org/10.1109/TPEL.2015.2429595

Dujic, D., Jones, M., Levi, E., *et al.*, 2011. Switching ripple characteristics of space vector PWM schemes for five-phase two-level voltage source inverters—Part 1: flux harmonic distortion factors. *IEEE Trans. Ind. Electron.*, **58**(7):2789-2798. https://doi.org/10.1109/TIE.2010.2070777

Duran, M.J., Barrero, F., 2016. Recent advances in the design, modeling and control of multiphase machines—part 2. *IEEE Trans. Ind. Electron.*, **63**(1):459-468. https://doi.org/10.1109/TIE.2015.2448211

Duran, M.J., Prieto, J., Barrero, F., 2013. Space vector PWM with reduced common-mode voltage for five-phase induction motor drives operating in over-modulation zone. *IEEE Trans. Power Electron.*, **28**(8):4030-4040. https://doi.org/10.1109/TPEL.2012.2229394

Ershad, N.F., Mirsalim, M., Aliabad, A.D., 2013. Line-start permanent magnet motors: proper design for pole-changing starting method. *IET Electr. Power Appl.*, **7**(6): 470-476. https://doi.org/10.1049/iet-epa.2012.0059

Gao, W.B., Wang, Y.F., Homaifa, A., 1995. Discrete-time variable structure control systems. *IEEE Trans. Ind. Electron.*, **42**(2):117-122. https://doi.org/10.1109/41.370376

Ge, B.M., Sun, D.S., Wu, W.L., 2013. Winding design, modeling, and control for pole-phase modulation induction motors. *IEEE Trans. Magn.*, **49**(2):898-911. https://doi.org/10.1109/TMAG.2012.2208652

Gregor, R., Barrero, F., Toral, S.L., *et al.*, 2010. Predictive space vector PWM current control method for asymmetrical dual three-phase induction motor drives. *IET Electr. Power Appl.*, **4**(1):26-34. https://doi.org/10.1049/iet-epa.2008.0274

Hoang, K.D., Ren, Y., Zhu, Z.Q., *et al.*, 2015. Modified switching-table strategy for reduction of current harmonics in direct torque controlled dual-three-phase permanent magnet synchronous machine drives. *IET Electr. Power Appl.*, **9**(1):10-19. https://doi.org/10.1049/iet-epa.2013.0388

Jiang, S.Z., Chau, K.T., Chan, C.C., 2003. Spectral analysis of a new six-phase pole-changing induction motor drive for electric vehicles. *IEEE Trans. Ind. Electron.*, **50**(1):123-131. https://doi.org/10.1109/TIE.2002.807662

Jones, M., Satiawan, N.W., Bodo, N., *et al.*, 2012. A dual five-phase space-vector modulation algorithm based on the decomposition method. *IEEE Trans. Ind. Appl.*, **48**(6): 2110-2120. https://doi.org/10.1109/TIA.2012.2226422

Kelly, J.W., 2007. A Novel Control Scheme for a Pole-Changing Induction Motor Drive. PhD Thesis, Michigan State University, East Lansing, MI.

Kelly, J.W., Strangas, E.G., 2007. Torque control during pole-changing transition of a 3:1 pole induction machine. Proc. Int. Conf. on Electrical Machines and Systems, p.1723-1728.

Lee, J.D., Khoo, S., Wang, Z.B., 2013. DSP-based sliding-mode control for electromagnetic-levitation precise-position system. *IEEE Trans. Ind. Inform.*, **9**(2):817-827. https://doi.org/10.1109/TII.2012.2219062

Levi, E., 2008. Multiphase electric machines for variable-speed applications. *IEEE Trans. Ind. Electron.*, 55(5): 1893-1909. https://doi.org/10.1109/TIE.2008.918488

Levi, E., 2016. Advances in converter control and innovative exploitation of additional degrees of freedom for multi-

phase machines. *IEEE Trans. Ind. Electron*., **63**(1):433-448. https://doi.org/10.1109/TIE.2015.2434999

Levi, E., Bojoi, R., Profumo, F., *et al.*, 2007. Multiphase induction motor drives—a technology status review. *IET Electr. Power Appl.*, **1**(4):489-516. https://doi.org/10.1049/iet-epa:20060342

Levi, E., Barrero, F., Duran, M.J., 2016. Multiphase machines and drives—revisited. *IEEE Trans. Ind. Electron.*, **63**(1): 429-432. https://doi.org/10.1109/TIE.2015.2493510

Li, F.H., Chau, K.T., Liu, C.H., 2016. Pole-changing flux-weakening DC-excited dual-memory machines for electric vehicles. *IEEE Trans. Energy Conv.*, **31**(1):27-36. https://doi.org/10.1109/TEC.2015.2479458

Lipo, T.A., 1994. Analysis of concentrated winding induction machines for adjustable speed drive applications—experimental results. *IEEE Trans. Energy Conv.*, **9**(4): 695-700. https://doi.org/10.1109/60.368339

Lipo, T.A., White, J.C., 1991a. Analysis of a concentrated winding induction machine for adjustable speed drive applications: part 1 (motor analysis). *IEEE Trans. Energy Conv.*, **6**(4):679-683. https://doi.org/10.1109/60.103641

Lipo, T.A., White, J.C., 1991b. Analysis of a concentrated winding induction machine for adjustable speed drive applications: part 2 (motor design and performance). *IEEE Trans. Energy Conv.*, **6**(4):684-692. https://doi.org/10.1109/60.103642

Luis, S.I., 2014. Space phases theory and control of multiphase machines through their decoupling into equivalent three-phase machines. *Electr. Eng.*, **96**(1):79-94. https://doi.org/10.1007/s00202-013-0278-6

Martin, J., Dujic, D., Levi, E., *et al*., 2011. Switching ripple characteristics of space vector PWM schemes for five-phase two-level voltage source inverters—part 2: current ripple. *IEEE Trans. Ind. Electron*., **58**(7):2799-2808. https://doi.org/10.1109/TIE.2010.2070778

Mengoni, M., Zarri, L., Gritli, Y., *et al*., 2015. Online detection of high-resistance connections in multiphase induction machines. *IEEE Trans. Power Electron*., **30**(8):4505-4513. https://doi.org/10.1109/TPEL.2014.2357439

Osama, M., Lipo, T.A., 1997. Modeling and analysis of a wide-speed-range induction motor drive based on electrical pole changing. *IEEE Trans. Ind. Appl.*, **33**(5):1177-3184. https://doi.org/10.1109/IAS.1996.557047

Shi, L.W., Zhou, B., 2016. Analysis of a new five-phase fault-tolerant doubly salient brushless DC generator. *IET Electr. Power Appl.*, **10**(7):633-640. https://doi.org/10.1049/iet-epa.2015.0589

Subotic, I., Bodo, N., Levi, E., *et al.*, 2016. Overview of fast on-board integrated battery chargers for electric vehicles based on multiphase machines and power electronics. *IET Electr. Power Appl.*, **10**(3):217-229. https://doi.org/10.1049/iet-epa.2015.0292

Tian, M.M., Wang, X.H., Li, G.Q., 2016. Line-start permanent magnet synchronous motor starting capability improvement using pole-changing method. 11th Conf. on Industrial Electronics and Applications, p.479-483.

Tuan, D.M., Man, Z.H., Zhang, C.S., *et al*., 2013. Robust sliding mode learning control for uncertain discrete-time multi-input multi-output systems. *IET Contr. Theory Appl.*, **8**:1045-1053. https://doi.org/10.1049/iet-cta.2013.0604

Utkin, V.I., 1977. Variable structure systems with sliding modes. *IEEE Trans. Autom. Contr.*, **22**(2):212-222. https://doi.org/10.1109/TAC.1977.1101446

Utkin, V.I., Guldner, J., Shi, J., 1999. Sliding Mode Control in Electromechanical Systems. Taylor & Francis, London.

Wang, D., Lin, H.Y., Yang, H., *et al.*, 2015. Design and analysis of a variable-flux pole-changing permanent magnet memory machine. *IEEE Trans. Magn.*, **51(**11):8113004. https://doi.org/10.1109/TMAG.2015.2448118

Wang, D., Lin, H.Y., Yang, H., *et al*., 2016a. Cogging torque optimization of flux memory pole-changing permanent magnet machine. *IEEE Trans. Appl. Supercond*., **26**(4): 0603105. https://doi.org/10.1109/TASC.2016.2535361

Wang, D., Lin, H.Y., Yang, H., *et al.*, 2016b. Design and investigation of a fractional slot pole-changing memory machine. 11th Int. Conf. on Ecological Vehicles and Renewable Energies, p.1-7. https://doi.org/10.1109/EVER.2016.7476408